Bimetallic Perthiocarbonate Complexes of Cobalt: Synthesis, Structure and Bonding

Alaka Nanda Pradhan, Shivankan Mishra, Urminder Kaur, Bikram Keshari Rout, Jean-François Halet, Sundargopal Ghosh

molecules

MDPI

Article

Bimetallic Perthiocarbonate Complexes of Cobalt: Synthesis, Structure and Bonding

Alaka Nanda Pradhan [1], Shivankan Mishra [1], Urminder Kaur [1], Bikram Keshari Rout [1], Jean-François Halet [2,*] and Sundargopal Ghosh [1,*]

[1] Department of Chemistry, Indian Institute of Technology Madras, Chennai 600036, India; salupradhan7@gmail.com (A.N.P.); shivankan1994@gmail.com (S.M.); urminderkaur27@gmail.com (U.K.); bikramrout44@gmail.com (B.K.R.)

[2] Univ Rennes, CNRS, École Nationale Supérieure de Chimie de Rennes, Institut des Sciences Chimiques de Rennes (ISCR)—UMR 6226, F-35000 Rennes, France

* Correspondence: jean-francois.halet@univ-rennes.fr (J.-F.H.); sghosh@iitm.ac.in (S.G.); Tel.: +91-44-225-742-30 (S.G.)

Abstract: The syntheses and structural elucidation of bimetallic thiolate complexes of early and late transition metals are described. Thermolysis of the bimetallic hydridoborate species [{Cp*CoPh}{μ-TePh}{μ-TeBH$_3$-κ^2Te,H}{Cp*Co}] (Cp* = η^5-C$_5$Me$_5$) (**1**) in the presence of CS$_2$ afforded the bimetallic perthiocarbonate complex [(Cp*Co)$_2$(μ-CS$_4$-κ^1S:κ^2S′)(μ-S$_2$-κ^2S″:κ^1S‴)] (**2**) and the dithiolene complex [(Cp*Co)(μ-C$_3$S$_5$-κ^1S,S′] (**3**). Complex **2** contains a four-membered metallaheterocycle (Co$_2$S$_2$) comprising a perthiocarbonate [CS$_4$]$^{2-}$ unit and a disulfide [S$_2$]$^{2-}$ unit, attached opposite to each other. Complex **2** was characterized by employing different multinuclear NMR, infrared spectroscopy, mass spectrometry, and single-crystal X-ray diffraction studies. Preliminary studies show that [Cp*VCl$_2$]$_3$ (**4**) with an intermediate generated from CS$_2$ and [LiBH$_4$·THF] yielded thiolate species, albeit different from the cobalt system. Furthermore, a computational analysis was performed to provide insight into the bonding of this bimetallic perthiocarbonate complex.

Keywords: chalcogen; cobalt; perthiocarbonate; sulfur; trithiocarbonate; vanadium

Citation: Pradhan, A.N.; Mishra, S.; Kaur, U.; Rout, B.K.; Halet, J.-F.; Ghosh, S. Bimetallic Perthiocarbonate Complexes of Cobalt: Synthesis, Structure and Bonding. *Molecules* **2024**, *29*, 2688. https://doi.org/10.3390/molecules29112688

Academic Editors: Andrea Bencini and Vito Lippolis

Received: 3 May 2024
Revised: 23 May 2024
Accepted: 2 June 2024
Published: 6 June 2024

1. Introduction

The efficiency of metal sulfides as heterogeneous catalysts and the activity of metalloproteins in enzyme-mediated catalysis are generally significantly impacted by the nature of the metal–sulfur entities. An intriguing and unusual structural chemistry became apparent via a systematic search for metal–sulfur types of compounds given the variety of coordination possibilities that sulfur ligands can provide [1,2]. Indeed, CS$_2$ ligands have been shown to be versatile synthetic reagents ever since the first transition metal–CS$_2$ complexes were synthesized in 1967 [3] due to their electron donating and electron accepting properties, yielding an array of binding modes with one or more transition metal atoms [4–6].

In this context, Jagirdar's group demonstrated the insertion of CS$_2$ into one of the Ir-H bonds in [Ir(H)$_5$(PCy$_3$)$_2$] to afford the dihydrido dithioformate complex *cis*-[Ir(H)$_2$(η^2-S$_2$CH)(PCy$_3$)$_2$] (**A**), accompanied by the elimination of H$_2$ [7]. Similarly, the cyclometalated ruthenium complex [Ru(S$_2$C(H)PMe$_2$CH$_2$-κ^3S,S,C)(PMe$_3$)$_3$] was shown to react with an excess of CS$_2$, which undergoes a second insertion into a Ru–S bond to yield [Ru(SC(=S)SCH(–S)PMe$_2$CH$_2$-κ^3S,S,C)(PMe$_3$)$_3$] (**B**) [8]. Wang and coworkers reported the disproportionation of CS$_2$ when reacted with the Me$_2$C and Me$_2$Si doubly bridged bis(cyclopentadienyl) dinuclear molybdenum carbonyl complex (Me$_2$C)(Me$_2$Si)[(η^5-C$_5$H$_3$)Mo(CO)$_3$]$_2$, which led to the formation of complex **C** [9]. Likewise, in 2021, Fischer's group showcased that the nucleophilicity of the monodithiolene species [Mo(CO)$_2$(dt)(dppe)] (dt: cydt = cyclohex-1-ene-1,2-dithiol or tpydt = 5,6-dihydro-2H-thiopyran-3,4-dithiol, dppe = 1,2-bis(diphenylphosphino)

ethane) can be switched on by reduction with 2 eq. of [Co(Cp*)$_2$] in a mixture of DCM and ACN, which leads to the isomorphic complexes [Mo(CO)$_2$(CH$_2$-dt)(dppe)] (dt = cydt (**D**); dt = tpydt (**D′**)), with molybdenum formally in the zero oxidation state [10]. In addition, Bianchini's group showcased the nucleophilic nature of η^2-CS$_3$, where the trithiocarbonate complex of cobalt [Co(tppme)(S$_2$CS)] (tppme = 1.1.1-tris(diphenylphosphinomethyl)ethane) was reacted with [Cr(CO)$_5$·THF], resulting in the formation of **E** [11]. Recently, our group has reported the reaction of *arachno*-ruthenaborane [(Cp*Ru)$_2$(B$_3$H$_8$)(CS$_2$H)] with group 6 metal carbonyls [M(CO)$_5$·THF] (M = Mo and W), which led to the formation of methanedithiolato-bridged hetero-trimetallic complexes, namely [{Cp*Ru(CO)}$_2$(μ-CO)$_2$(μ_3-CH$_2$S$_2$-κ^2S′:κ^2S″){M(CO)$_2$}] (M = Mo and W) (**F**) [12] (Chart 1).

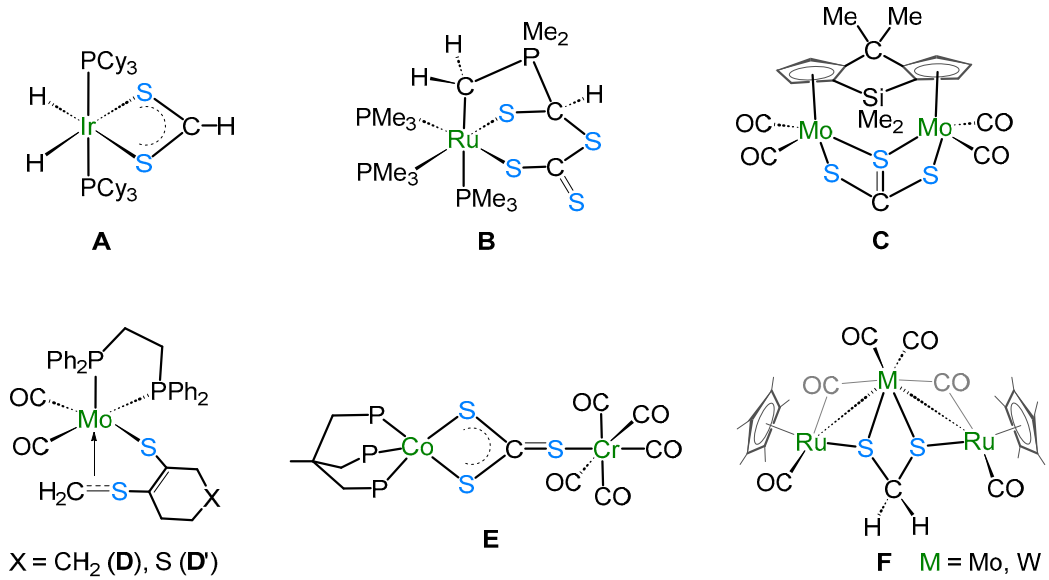

Chart 1. Different binding modes of CS$_2$-based ligands (**A**–**F**) in transition metal complexes.

Over the last few decades, we and others have synthesized interesting polyhedral clusters, both single-cage and fused, employing early and late transition metals [13–18]. Despite being largely uncontrolled, the isolation of numerous unique metallaheteroboranes demonstrating novel coordination modes prompted us to investigate this area more meticulously. In this context, our group utilized three distinct strategies: (i) pentamethylcyclopentadienyl-based metal halides with chalcogen-based borate ligands such as [LiBH$_2$E$_3$], [LiBH$_3$EPh] (E = S, Se, Te), [LiBH$_4$ + CS$_2$], or [NaBH$_4$ + CS$_2$] [19–21]; (ii) preformed metallaboranes with the above chalcogen-based borate ligands [21]; and (iii) preformed metallaboranes with CS$_2$ or CS$_2$-based ligands such as [CS$_2$·PPh$_3$] [22,23]. In our earlier reports, the classical diborane [B$_2$H$_5$]$^-$ was stabilized by the reaction of [Cp*TaCl$_4$] with [LiBH$_4$·THF], followed by the addition of excess [S$_2$C·PPh$_3$] adduct [23]. Also, these chalcogen-based borate ligands have been utilized for cluster expansion reactions. The reactivity of *nido*-[(Cp*M)$_2$B$_6$H$_{10}$] (M = Co and Rh) with the chalcogen-based borate Li[BH$_2$E$_3$] (E = S, Se, or Te) afforded 10-vertex *nido*-dimetallaheteroborane clusters [21]. By using a different chalcogen-based ligand (intermediate generated from CS$_2$ and [LiBH$_4$·THF]) with *nido*-[(Cp*M)$_2$B$_6$H$_{10}$] (M = Co and Rh), unique dimetalladecaborane(14) analogues containing di(thioboralane)-thione {B$_2$CS$_3$} and di(thioborolane) {B$_2$S$_2$CH$_2$} moieties were isolated [21]. Very recently, the reactivity of a borate ligand derived from CS$_2$ with κ^2-N,S-chelated ruthenium borate complexes, [Ph$_3$P(κ^2-N,S-L)Ru{κ^3-H,S,S′-H$_2$B(L)$_2$}] (L = C$_7$H$_4$NS$_2$, C$_5$H$_4$NS), has been investigated [24]. Therefore, we pursued this chemistry, reacting the cobalt borate complex [{Cp*CoPh}{μ-TePh}{μ-TeBH$_3$-κ^2Te,H}{Cp*Co}] (**1**) [19] with CS$_2$. Although the objective of obtaining transition metal complexes containing boron content was not achieved, interesting cobalt and vanadium thiolate complexes were isolated.

2. Results and Discussion

2.1. Reactivity of **1** *with* CS_2

Transition metal–chalcogen complexes are well documented in the literature. Recently, we have shown that the reaction of $[Cp^*Ru(\mu\text{-}Cl)Cl]_2$ with $Na[BH_3(SCHS)]$ led to the formation of several bimetallic dithioformato ruthenium complexes, where the dithioformate ligand (CH_2S_2) shows diverse binding modes with the metal center(s) [20]. In addition, the reaction of $[1,2\text{-}(Cp^*Ru)_2(\mu\text{-}H)_2B_3H_7]$ with CS_2 yielded the *arachno*-ruthenaborane $[(Cp^*Ru)_2(B_3H_8)(CS_2H)]$, with a dithioformato ligand attached to it by the metal-assisted hydroboration [22]. Thus, investigation of the CS_2 ligand with transition metal boron species became of interest. With this background, we reacted **1** with CS_2 under thermolytic condition. Thus the reaction of **1** with CS_2 under thermolytic conditions. The reaction of **1** with CS_2 in toluene at 70 °C for 6 h led to the formation of an air-stable complex, the brown solid **2** (18% yield, R_f = 0.46), and the known green dithiolene complex $[(Cp^*Co)(\mu\text{-}C_3S_5\text{-}\kappa^1S\text{:}\kappa^1S')]$ **3** [25] (12% yield, R_f = 0.58) (Scheme 1). The identification of complex **2** was confirmed by combined ^1H, $^{13}C\{^1H\}$ NMR, IR spectroscopy, mass spectrometry, and single-crystal X-ray diffraction studies. The detailed characterization of complex **2** is discussed below.

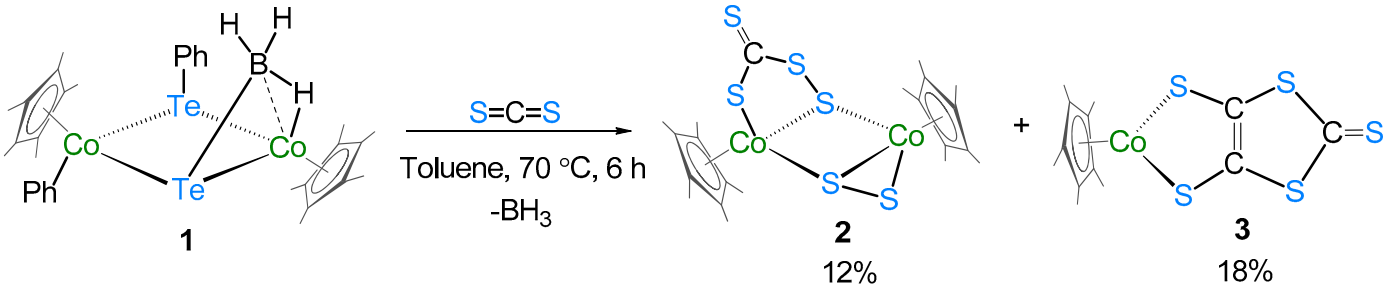

Scheme 1. Synthesis of the perthiocarbonate (**2**) and dithiolene (**3**) complexes of cobalt.

The ^{11}B NMR of complex **2** shows no chemical shifts, and the ^1H NMR spectrum shows no upfield region peaks, which rules out the possibility of the formation of a boron-containing complex. Indeed, complex **2** is formed by the release of BH_3 from complex **1**. We confirmed the release of the $[BH_3{\cdot}PPh_3]$ adduct by trapping it with PPh_3. The $^{11}B\{^1H\}$ and $^{31}P\{^1H\}$ NMR spectra (Figures S7 and S8) of the reaction mixture show resonances at $\delta = -39.3$ and 20.8 ppm, respectively. The ^1H NMR spectrum displays two resonances at δ = 1.38 and 1.63 ppm at a 1:1 ratio, corresponding to Cp* ligands. The presence of two different Cp* ligands is also supported by the $^{13}C\{^1H\}$ NMR spectrum. In addition to Cp* peaks, the $^{13}C\{^1H\}$ NMR shows resonance at δ = 252.7 ppm, which indicates the presence of a C=S moiety. The infrared spectrum shows a peak at 1020 cm^{-1} that confirms the presence of this C=S double bond. Further, the mass spectrometric analysis of **2** shows an isotopic pattern (ESI^+ mode) at m/z = 592.9376, which corresponds to the molecular formula $C_{21}H_{31}Co_2S_6$. Although all the spectroscopic and mass spectrometric data point toward the formation of a thiolate complex, the solid-state framework of **2** was confirmed by single-crystal X-ray diffraction studies. The crystals were grown by slow evaporation of an *n*-hexane/CH_2Cl_2 (30:70) solution at 5 °C.

The solid-state X-ray structure of complex **2** shows the bimetallic perthiocarbonate complex $[(Cp^*Co)_2(\mu\text{-}CS_4\text{-}\kappa^1S\text{:}\kappa^2S')(\mu\text{-}S_2\text{-}\kappa^2S''\text{:}\kappa^1S''')]$ (Figure 1). Note that there are two molecules in the asymmetric unit. To the best of our knowledge, complex **2** is the first structurally characterized perthiocarbonate complex of cobalt. It consists of a four-membered metallaheterocycle (Co_2S_2) comprising a rare perthiocarbonate $[CS_4]^{2-}$ unit and a disulfide $[S_2]^{2-}$ unit, attached opposite to each other. The bidentate $[CS_4]^{2-}$ fragment bridges two {CoCp*} moieties in a $\mu_2\text{-}\eta^2$ fashion. Complex **2** represents, in turn, a novel type of structure having both perthiocarbonate anion $[CS_4]^{2-}$ and disulfide $[S_2]^{2-}$ units, with 18-electron

cobalt (III) centers. Note that Adams' group previously showed that the disulfur unit is a potential candidate for disulfur/dithiolate conversion [26,27].

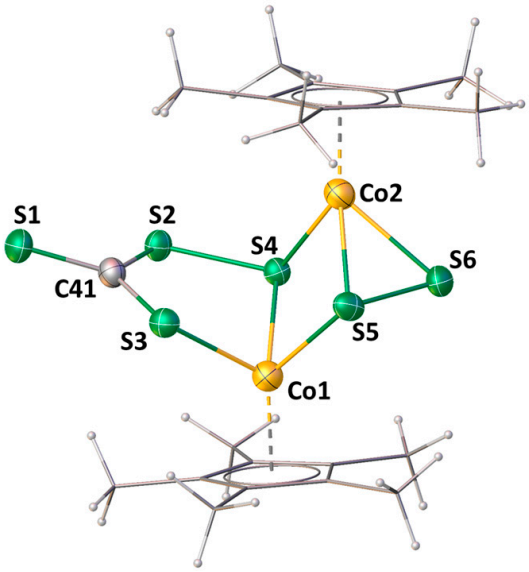

Figure 1. Molecular structure and labeling diagram of **2**. Selected bond lengths (Å) and bond angles (°): Co1–S4 2.200(3), Co1–S3 2.264(4), S5–S6 2.043(14), Co2–S5 2.202(4), Co2–S6 2.258(15), Co1···Co2 3.332, C41–S1 1.663(10), C41–S2 1.724(12), C41–S3 1.722(10), S2–S4 2.080(4), S3–C41–S2 119.3(6), Co1–S4–Co2 95.97(12), S4–Co1–S5 83.08(13), S5–Co2–S6 54.5(4), Co2–S5–Co1 96.91(13), S5–S6–Co2 61.4(4).

The average Co–S bond length of 2.242 Å is comparable to that in cobalt–thiolate complexes [28,29], and the average bridged Co–S distance of 2.233 Å is slightly shorter than the unbridged Co–S bonds (2.261 Å). Further, the Co···Co distance of 3.332 Å clearly suggests the absence of any metal–metal (Co–Co) bond, making it a coordinatively saturated 18-electron species. Transition metal–perthiocarbonate complexes are well documented in the literature, in which the $[CE_4]^{2-}$ ion (E = S, Se) acts as a 1,1′-dithiolate ligand. Some examples of such complexes are listed in Table 1 [30–33], which describe the different bonding modes, structural parameters, and spectroscopic data of complexes with $[CE_4]^{2-}$ units.

Generally, the perthiocarbonate anion, $[CS_4]^{2-}$, is obtained by the reaction of CS_2 with disulfide or polysulfide dianions. Perthiocarbonate complexes can be synthesized from trithiolate complexes $[M(CS_3)_2]^{2-}$ by I_2 oxidation or the addition of sulfur [34]. Shieh and co-workers reported the first example of $[CE_4]^{2-}$ incorporated into transition metal–carbonyl complexes, $[(CE_4)_2Mn_2(CO)_6]^{2-}$ (E = S, Se) (Table 1) [32], where two $[CE_4]^{2-}$ fragments were connected to two $\{Mn(CO)_3\}$ units symmetrically. In the case of complex **2**, only one $[CS_4]^{2-}$ unit is present. In this $[CS_4]^{2-}$ unit, the bond distance C41–S1 (1.663(10) Å) is a bit shorter than C41–S3 (1.722(10) Å) and C41–S2 (1.724(12) Å) and indicates a double-bond character. In **3**, the double-bond character of C=S (1.657(7) Å) is slightly more pronounced than in **2** (1.663(10) Å). On the other hand, the four-electron donor disulfide ligand is coordinated to two cobalt centers in η^1,η^2-S_2 mode, similar to $[(Cp^*Co)_2(\eta^1,\eta^2\text{-}S_2)_2]$ [35], $[(Cp^*Ru)_2(\eta^1,\eta^2\text{-}S_2)(\eta^1,\eta^1,\eta^1\text{-}S_3)]$ [36], and $[(triphos)_2Rh_2(\eta^1,\eta^2\text{-}Se_2)_2][PPh_4]_2$ (triphos = $H_3CC(CH_2PPh_2)_3$) [37]. The S–S distance of 2.043(14) Å in **2** is comparable to the S–S distances measured in $[(Cp^*Co)_2(\eta^1,\eta^2\text{-}S_2)_2]$ (2.062(6) Å) [35] and $[(Cp^*Ru)_2(\eta^1,\eta^2\text{-}S_2)(\eta^1,\eta^1,\eta^1\text{-}S_3)]$ (1.907(5) Å) [36].

Table 1. Selected structural parameters and spectroscopic data of transition metal complexes featuring perthiocarbonate moiety $[CE_4]^{2-}$.

Bonding Modes of $[CE_4]^{2-}$		Structural Parameters			$^{13}C\{^1H\}$ [b]	ν_{CE} (cm^{-1})
		d_{C-E} (Å) [a]	$d_{C=E}$ (Å) [a]	∠E-C-E (°)		
$[\eta^2]$	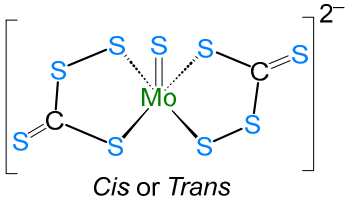 *Cis* or *Trans*	1.73 1.71	1.59 (*cis*) 1.65 (*trans*)	118.3 (*cis*) 119.6 (*trans*)	245.6 246.0	977 (*cis*) 980 (*trans*)
	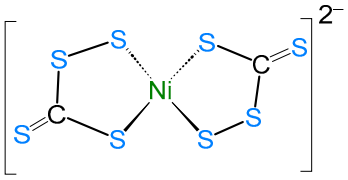	1.71	1.67	120.2	na	na
	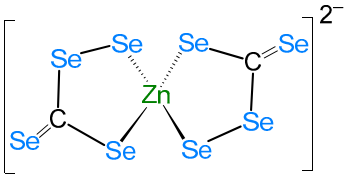	1.85	1.81	124.0	na	na
$[\mu_2\text{-}\eta^2]$	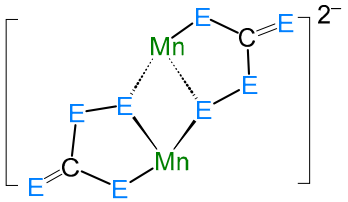 Mn = $Mn(CO)_3$, E = S, Se	1.72 (S) 1.85 (Se)	1.67 (S) 1.81 (Se)	120.8 (S) 122.5 (Se)	na	na
	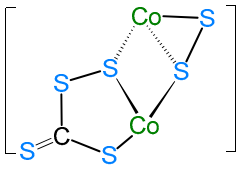 Co = Cp*Co **2**	1.72	1.663(10)	119.2	252.7	1020

[a] Average distance. [b] In ppm. na = Not available.

DFT theoretical calculations were carried out for insight into the electronic structure and bonding situation in **2** (see Section 3.3 for the computational details). The molecular orbital (MO) analysis of **2** shows a large HOMO-LUMO energy gap of 3.19 eV. Among the important MOs, the HOMO-12 of **2** shows a large *d* (M)-*p* (S) interaction of atom Co2 with the sulfur atoms of the disulfur unit (Co2–S5 and Co2–S6) (Figure 2a). Moreover, the HOMO-26 of **2** depicts the S–S end-to-end σ-bonding interaction of the disulfur unit, which is also confirmed by the contour line diagram (Figure 2c,d). The HOMO-26 also shows a side-to-side overlap of the *p* orbitals of C41–S1 (π-interaction). This double-bond character is also reflected by a higher Wiberg bond index (WBI) computed for C41–S1 (1.585 Å) and a shorter calculated bond distance of 1.652 Å. On the other hand, the HOMO-17 of **2** shows the σ-bonding interaction of the $[CS_4]$ unit (Figure 2b). Overall, the contour line diagram reveals the CS_3 bonding interaction in the S1–C41–S2–S3 plane, which also indicates the sp^2 character of the atom C41 (Figure 2e).

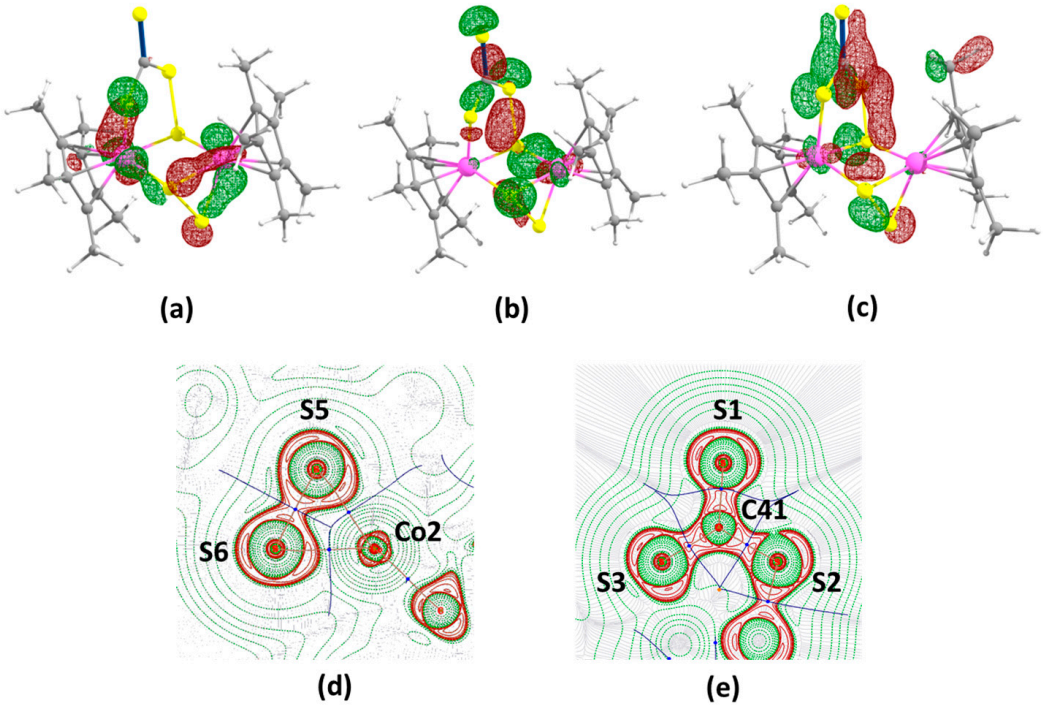

Figure 2. (**a**) HOMO-12, (**b**) HOMO-17, and (**c**) HOMO-26 of **2**. Contour isodensity values for isosurface are ± 0.045 $(e/bohr^3)^{1/2}$. (**d**,**e**), Laplacian maps of the electron density distribution computed for **2** in the Co2–S5–S6 plane and the S1–S2–S3 plane, respectively.

In the recent past, we isolated and structurally characterized paramagnetic thiocarbonate complexes from the reaction of $Na_5[B(CH_2S_2)_4]$ and $[Cp^*VCl_2]_3$ (**4**) [38]. Thus, with the objective of isolating similar types of thiolate complexes to that of complex **2**, we explored the reactivity of $[Cp^*VCl_2]_3$ (**4**) with an intermediate generated from CS_2 and $[LiBH_4{\cdot}THF]$ under different reaction conditions, which yielded the inseparable yellow solids **5** and **6** (Scheme S1). Although we do not have detailed characterizations of these inseparable complexes, preliminary studies (X-ray diffraction analysis) show that **5** and **6** are binuclear vanadium trithiocarbonate $[(Cp^*V)_2(\mu\text{-}CS_3\text{-}\kappa^2S,S')_2]$ and (disulfaneyl)methanethiolate $[(Cp^*V)_2(\mu\text{-}SCH_2S_2\text{-}\kappa^2S,S')_2]$ complexes, respectively (Figures S1 and S2).

2.2. UV–vis Study of **2**

The absorption patterns of the colored complex **2** may be of interest due to the presence of different chalcogen fragments. Therefore, the UV–vis absorption spectrum of **2** was measured in the range of 280–800 nm in CH_2Cl_2 solution at 298 K (Figure 3). In fact, the most intense peaks in the higher-energy regions (280–320 nm) are due to the spin-allowed π–π* transition of the Cp* ligands present in these complexes [39]. Comparatively low-intensity peaks at a lower energy around 320–550 nm may be due to the charge transfer bands. In order to obtain more detail, time-dependent DFT calculations were carried out on **2**. In complex **2**, the high-intensity absorption band near 326 nm is due to the HOMO–6→LUMO electronic transition. The HOMO-6 is mostly from metal-based *d* orbitals, while the LUMO has both metal (*d* orbital) and disulfide $[S]^{2-}$ (*p* orbital on S atoms) orbital characters (Figure S10). Therefore, these absorption bands can be assigned as metal-to-ligand charge transfer (MLCT) transitions. In the low-energy wavelength region, **2** shows a low-intensity absorption band at 570 nm, which could be due to the intramolecular LMCT transitions.

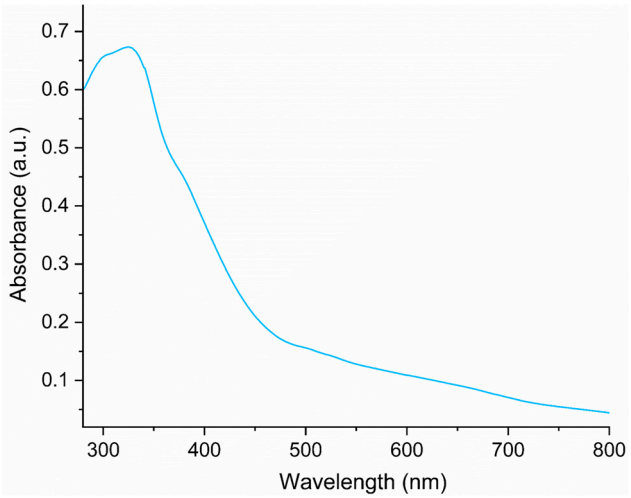

Figure 3. UV–vis spectrum of **2** in CH_2Cl_2.

2.3. Electrochemical Study of **2**

The redox properties of complex **2** dissolved in DMF were examined using cyclic voltammetry (Figure 4). The DMF solution displays two irreversible responses at E_{pc} = −1.47 V and −0.86 V vs. Fc/Fc^+. They may originate from the reduction of the disulfide or metal-centered reduction based on the reported literature. The two irreversible anodic responses at E_{pa} = 0.11 V and 0.27 V vs. Fc/Fc^+ are most likely due to the oxidation of the thiolate ligand [40–44].

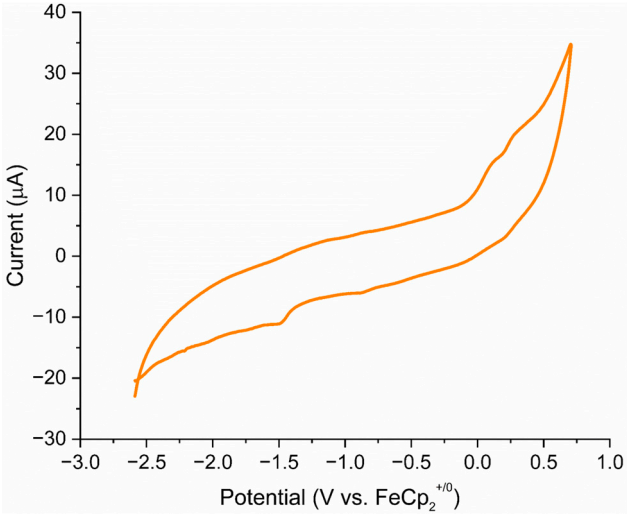

Figure 4. Cyclic voltammogram (CV) recorded for complex **2** in DMF at 298 K.

3. Materials and Methods

3.1. General Procedures and Instrumentation

All the experimental procedures were performed in an argon atmosphere by using standard Schlenk line techniques and a glove box. All the solvents, *n*-hexane, DCM (dichloromethane), toluene, and THF (tetrahydrofuran), were distilled under an argon atmosphere prior to use. All the chemicals, such as Ph_2Te_2 (diphenyl ditelluride) (Sigma Aldrich, Bangalore, India) and CS_2 (Loba Chemie Pvt. Ltd., Mumbai, India), were purchased and used as received. The complexes [{Cp*CoPh}{μ-TePh}{μ-TeBH$_3$-κ^2Te,H}{Cp*Co}] (**1**) [19] and $[Cp^*VCl_2]_3$ (**4**) [45] were prepared according to the methods from the literature. Dialuminum-supported TLC plates (MERCK TLC plates, Bangalore, India) were used for the separation of the reaction mixtures. All the NMR spectra for the synthesized complexes were obtained on 500 MHz Bruker FT-NMR spectrometers, Billerica, MA, USA. The

residual solvent protons ($CDCl_3$, δ = 7.26 ppm) and carbons ($CDCl_3$, δ = 77.1 ppm) were employed as references for the ^1H and $^{13}C\{^1H\}$ NMR spectra, respectively. The mass data of all the synthesized complexes were recorded on Q-Tof Micro YA263 HRMS, Milford, MA, USA and 6545 Q-Tof LC/MS instruments, Santa Clara, CA, USA. The IR spectrum of **2** was recorded in dichloromethane solvent with a JASCO FT/ IR-1400 spectrometer, Easton, MD, USA. The UV–vis spectrum was recorded on a JASCO V-650 spectrometer, Tokyo, Japan. The cyclic voltammetry measurement was performed on an OrigaLys potentiostat, Rillieux-la-Pape, France in a standard three-electrode system (glassy carbon working electrode, platinum wire counter electrode, and Ag/Ag^+ as pseudo reference electrode). For deoxygenation, argon was bubbled into the electrolyte medium for 10 min. The cyclic voltammograms were recorded at a scan rate of 50 mVs^{-1}.

Synthesis of 2. In a pre-dried Schlenk tube, **1** (0.10 g, 0.123 mmol) was suspended in 10 mL of toluene. Under the atmosphere of argon, CS_2 (4 mL) was added slowly using a syringe at room temperature to the green solution of complex **1**. Then, the reaction mixture was kept at 70 °C (temperature of oil bath) for 6 h with continuous stirring under an atmosphere of argon. The solvent was removed by vacuum, and the remaining residue was separated and purified using the TLC method on silica gel TLC plates. Elution with *n*-hexane/CH_2Cl_2 (30:70 *v*/*v*) yielded the brown complex **2** (0.014 g, 18%) and the known green complex [(Cp*Co)(μ-C_3S_5-κ^1S:κ^1S′] **3** (0.012 g, 12%) [25].

2: MS (ESI^+) calcd. for $C_{21}H_{31}Co_2S_6^+$ $[M+H]^+$ *m*/*z* 592.9414, found 592.9376; ^1H NMR ($CDCl_3$, 500 MHz, 22 °C): δ = 1.38 (s, 15H; 1 × Cp*), 1.63 ppm (s, 15H; 1 × Cp*); $^{13}C\{^1H\}$ NMR ($CDCl_3$, 125 MHz, 22 °C): δ = 9.1, 10.0 (s, $C_5\underline{Me}_5$), 92.4, 94.9 (s, $\underline{C}_5Me_5$), 252.7 (C=S) ppm; IR (CH_2Cl_2): $\widetilde{\nu}$ = 1020 cm^{-1} (C=S); UV–vis [CH_2Cl_2, λ, nm]: 326, 384, and 570.

3.2. Single Crystal X-ray Diffraction Analysis

Suitable X-ray-quality crystals of **2** and **5**/**6** were grown by slow diffusion of an *n*-hexane/CH_2Cl_2 solution at 5 °C. The crystal data were collected and integrated using a Bruker D8 VENTURE diffractometer (Billerica, MA, USA) with a PHOTON 100 CMOS detector (Tokyo, Japan) for **2** and a Bruker AXS Kappa APEX2 CCD diffractometer (Billerica, MA, USA) for **5** and **6** with graphite monochromated Mo-*K*α (λ = 0.71073 Å) radiation at 293(2) K. The structures of these complexes were solved by heavy atom methods using *SHELXS-97* [46] and *SHELXT-2014* and refined using *SHELXL-2014*, *SHELXL-2017*, and *SHELXL-2018* [47]. All the molecular structures were drawn using *Olex2* [48]. Note that complexes **5** and **6** co-crystallize in the same crystallographic unit with disorder mainly over the sulfur and carbon atoms, with 0.56 and 0.44 occupancies, respectively. The crystal structure of **6** is further disordered over two components with a site occupancy ratio of 0.31:0.13. The crystallographic data were deposited with the Cambridge Crystallographic Data Centre as supplementary publication, nos. CCDC–2111767 (**2**) and 2349360 (**5** and **6**). These data can be obtained free of charge from the Cambridge Crystallographic Data Centre via www.ccdc.cam.ac.uk/data_request/cif access on 18 April 2024.

Crystal data for **2**: $C_{21}H_{30}Co_2S_6$, M_r = 592.67, monoclinic, space group $P2_1/n$, unit cell, a = 10.4689(14) Å, b = 32.997(5) Å, c = 14.971(2) Å, α = 90°, β = 99.029(10)°, γ = 90°, Z = 8, V = 5107.6(12) $Å^3$, μ = 14.806 mm^{-1}, $F(000)$ = 2448, ρ_{cacld} = 1.541 g/cm^3, R_1 = 0.0883, wR_2 = 0.2689, 8461 independent reflections [$2\theta \leq 64.999°$] and 672 parameters.

Crystal data for **5** and **6**: 0.56 ($C_{22}H_{30}S_6V_2$) + 0.44 ($C_{22}H_{34}S_6V_2$), M_r = 590.42, monoclinic, space group C2/*c*, unit cell, a = 18.6613(7) Å, b = 9.5327(4) Å, c = 16.0532(6) Å, α = 90°, β = 114.511(10)°, γ = 90°, Z = 4, V = 2598.39(18) $Å^3$, μ = 1.211 mm^{-1}, $F(000)$ = 1223, ρ_{cacld} = 1.509 g/cm^3, R_1 = 0.0392, wR_2 = 0.1066, 11180 independent reflections [$2\theta \leq 54.218°$] and 217 parameters.

3.3. Computational Details

Density functional theory (DFT) optimization of complex **2** was carried out using the *Gaussian 16 program* [49] with the B3LYP functional [50] and the def2-TZVP [51,52] basis set from the EMSL (Environmental Molecular Sciences Laboratory) Basis Set Exchange

Library. Complex **2** was thoroughly optimized without any solvent effect in the gaseous state, starting from its X-ray crystallographic structure. Frequency calculations were carried out to check the nature of the stationary state of **2** to confirm the absence of any imaginary frequency to confirm that it was an energy minimum on the potential energy hypersurface. A natural bonding analysis (NBO) was carried out with the NBO partitioning scheme [53–56], and Wiberg bond indexes [57] were obtained from it. A QTAIM [58–60] analysis was performed utilizing the *Multiwfn V.3.6* package [61]. The optimized structure and orbital graphics were produced using the *GaussView* (Version 3.09) [62] and *Chemcraft* (Version 1.8) [63] software.

4. Conclusions

In summary, we have isolated and structurally characterized a couple of bimetallic thiolate complexes of early and late transition metals featuring both partial and full reduction of the CS_2 moiety. One is a bimetallic cobalt thiolate complex which contains a perthiocarbonate group, as well as a disulfide group connected to two Co atoms in a μ_2-η^2 fashion. This complex displays an interesting coordination environment around the two homometallic centers. Investigations to evaluate the possibility of other early and late transition metal thiolate complexes with rare coordination modes are underway.

Supplementary Materials: The following supporting information can be downloaded at https://www.mdpi.com/article/10.3390/molecules29112688/s1. It contains ^{1}H, ^{13}C{^{1}H}, ^{11}B{^{1}H}, ^{31}P{^{1}H} NMR, IR, and mass spectra (Figures S3–S8), X-ray analysis details, and CIF and checkCIF files, as well as the xyz coordinates of the DFT-optimized cluster **2**, calculated HOMO and LUMO energy levels and HOMO-LUMO gaps, selected bond parameters, and Wiberg bond indices (WBI) for cluster **2** (Figures S10 and S11). All pulse sequences are available in a commercial Bruker spectrometer. ^{1}H decoupled ^{11}B spectra were processed with backward linear prediction algorithm to remove broad ^{11}B background signal from NMR probe and NMR tube. References [38,64–66] are cited in the supplementary materials.

Author Contributions: A.N.P. and U.K. formulated and planned the experiments; A.N.P., S.M., U.K. and B.K.R. carried out the synthesis and spectroscopic analyses and discussed the results with S.G. and J.-F.H.; A.N.P., S.M. and U.K. organized the manuscript with guidance from S.G. and J.-F.H.; S.G., supervision; S.G. and J.-F.H., project administration. All authors have read and agreed to the published version of the manuscript.

Funding: This work was supported by SERB, New Delhi, India, grant no. CRG/2023/000189.

Institutional Review Board Statement: Not applicable.

Informed Consent Statement: Not applicable.

Data Availability Statement: The original contributions presented in the study are included in the article/supplementary material, further inquiries can be directed to the corresponding author/s.

Acknowledgments: A.N.P. thanks UGC, India, for the research fellowship. S.M. and U.K. thank IIT Madras for the research fellowships. We thank Babu Varghese, P. K. Sudhadevi Antharjanam, and SAIF, IIT Madras, for the single-crystal X-ray data collection and structure analyses. The computational facilities of IIT Madras are gratefully acknowledged.

Conflicts of Interest: The authors declare no conflicts of interest.

References

1. Stiefel, E.I.; George, G.N. *Bioinorganic Chemistry*; Bertini, I., Gray, H.B., Lippard, S.J., Valentine, J.S., Eds.; University Science Books: Mill Valley, CA, USA, 1994.
2. Seo, W.T.M.; Tsui, E.Y. Structural and Redox Interconversions of Sulfur Ligands of Transition Metal Complexes. *Comment. Inorg. Chem.* **2024**, *44*, 55–97. [CrossRef]
3. Baird, M.C.; Wilkinson, G. Carbon disulphide, carbonyl sulphide, and alkyl and aryl isothiocyanate and perfluorothioacetone complexes of nickel, palladium, platinum, rhodium, and iridium. *J. Chem. Soc. A* **1967**, 865–872. [CrossRef]
4. Pandey, K.K. Reactivities of carbonyl sulfide (COS), carbon disulfide (CS_2) and carbon dioxide (CO_2) with transition metal complexes. *Coord. Chem. Rev.* **1995**, *140*, 37–114. [CrossRef]

5. Lou, J.; Wang, Q.; Wu, P.; Wang, H.; Zhou, Y.-G.; Yu, Z. Transition-metal mediated carbon–sulfur bond activation and transformations: An update. *Chem. Soc. Rev.* **2020**, *49*, 4307–4359. [CrossRef] [PubMed]
6. Wang, L.; Hea, W.; Yu, Z. Transition-metal mediated carbon–sulfur bond activation and transformations. *Chem. Soc. Rev.* **2013**, *42*, 599–621. [CrossRef]
7. Nanishankar, H.V.; Dutta, S.; Nethaji, M.; Jagirdar, B.R. Dynamics of a *cis*-Dihydrogen/Hydride Complex of Iridium. *Inorg. Chem.* **2005**, *44*, 6203–6210. [CrossRef] [PubMed]
8. Field, L.D.; Jurd, P.M.; Magill, A.M.; Bhadbhade, M.M. Reactions of CO_2 and CS_2 with [RuH(η^2-CH_2PMe_2)(PMe_3)$_3$]. *Organometallics* **2013**, *32*, 636–642. [CrossRef]
9. Li, B.; Tan, X.; Xu, S.; Song, H.; Wang, B. Unexpected reactions of (Me_2C)(Me_2Si)[(η^5-C_5H_3)Mo(CO)$_3$]$_2$ with diazoalkane and carbon disulfide: Activation and cleavage of the N≡N bond and disproportionation of carbon disulfide. *J. Organomet. Chem.* **2008**, *693*, 667–674. [CrossRef]
10. Elvers, B.J.; Krewald, V.; Schulzke, C.; Fischer, C. Reduction induced S-nucleophilicity in mono-dithiolene molybdenum complexes–*in situ* generation of sulfonium ligands. *Chem. Commun.* **2021**, *57*, 12615–12618. [CrossRef]
11. Bianchini, C.; Mealli, C.; Meli, A.; Scapacci, G. Cobalt(II) and nickel(II) trithiocarbonate complexes as nucleophilic reagents. Reactivity and X-ray structure of the trithiocarbonate complex [Co(tppme)(S_2CSCH_3)][BPh_4]·1.5thf. *J. Chem. Soc. Dalton Trans.* **1982**, 799–804. [CrossRef]
12. Bairagi, S.; Giri, S.; Patel, D.K.; Luong, D.; Fokwa, B.P.T.; Ghosh, S. Hetero-trimetallic complexes comprising bridging boryl and borylene ligands: An experimental and theoretical study. *Dalton Trans.* **2024**, *53*, 3191–3205. [CrossRef]
13. Roy, D.K.; Mondal, B.; Anju, R.S.; Ghosh, S. Chemistry of Diruthenium and Dirhodium Analogues of Pentaborane(9): Synthesis and Characterization of Metal N, S-Heterocyclic Carbene and B-Agostic Complexes. *Chem. Eur. J.* **2015**, *21*, 3640–3648. [CrossRef] [PubMed]
14. Yuvaraj, K.; Roy, D.K.; Geetharani, K.; Mondal, B.; Anju, V.P.; Shankhari, P.; Ramkumar, V.; Ghosh, S. Chemistry of Homo- and Heterometallic Bridged-Borylene Complexes. *Organometallics* **2013**, *32*, 2705–2712. [CrossRef]
15. Mondal, B.; Bag, R.; Ghorai, S.; Bakthavachalam, K.; Jemmis, E.D.; Ghosh, S. Synthesis, Structure, Bonding, and Reactivity of Metal Complexes Comprising Diborane(4) and Diborene(2): [{Cp*Mo(CO)$_2$}$_2${μ-η^2:η^2-B_2H_4}] and [{Cp*M(CO)$_2$}$_2$$B_2H_2$M(CO)$_4$], M = Mo, W. *Angew. Chem. Int. Ed.* **2018**, *57*, 8079–8083. [CrossRef] [PubMed]
16. Ghosh, S.; Noll, B.C.; Fehlner, T.P. Expansion of iridaborane clusters by addition of monoborane. Novel metallaboranes and mechanistic detail. *Dalton Trans.* **2008**, 371–378. [CrossRef] [PubMed]
17. Sharmila, D.; Mondal, B.; Ramalakshmi, R.; Kundu, S.; Varghese, B.; Ghosh, S. First-row Transition Metal-Diborane and Borylene Complexes. *Chem. Eur. J.* **2015**, *21*, 5074–5083. [CrossRef] [PubMed]
18. Weller, A.S. d- and f-Block Metallaboranes. In *Comprehensive Organometallic Chemistry III*; Crabtree, R.H., Mingos, D.M.P., Eds.; Elsevier: Oxford, UK, 2007; Volume 3, pp. 133–174. [CrossRef]
19. Joseph, B.; Gomosta, S.; Prakash, R.; Roisnel, T.; Phukan, A.K.; Ghosh, S. Chalcogen Stabilized bis-Hydridoborate Complexes of Cobalt: Analogues of Tetracyclo[4.3.0.02,4.03,5]nonane. *Chem. Eur. J.* **2020**, *26*, 16824–16832. [CrossRef] [PubMed]
20. Saha, K.; Kaur, U.; Kar, S.; Mondal, B.; Joseph, B.; Antharjanam, P.K.S.; Ghosh, S. Trithia-diborinane and Bis(bridging-boryl) Complexes of Ruthenium Derived from a [BH_3(SCHS)]$^-$ Ion. *Inorg. Chem.* **2019**, *58*, 2346–2353. [CrossRef] [PubMed]
21. Pathak, K.; Nandi, C.; Ghosh, S. Metallaheteroboranes with group 16 elements: Aspects of synthesis, framework and reactivity. *Coord. Chem. Rev.* **2022**, *453*, 214303. [CrossRef]
22. Anju, R.S.; Saha, K.; Mondal, B.; Dorcet, V.; Roisnel, T.; Halet, J.-F.; Ghosh, S. Chemistry of Diruthenium Analogue of Pentaborane(9) With Hetero-cumulenes: Towards Novel Trimetallic Cubane-type Clusters. *Inorg. Chem.* **2014**, *53*, 10527–10535. [CrossRef] [PubMed]
23. Saha, K.; Ghorai, S.; Kar, S.; Saha, S.; Halder, R.; Raghavendra, B.; Jemmis, E.D.; Ghosh, S. Stabilization of Classical [B_2H_5]$^-$: Structure and Bonding of [(Cp*Ta)$_2$(B_2H_5)(μ-H)L_2] (Cp* = η^5-C_5Me_5; L = SCH_2S). *Angew. Chem. Int. Ed.* **2019**, *58*, 17684–17689. [CrossRef]
24. Ahmad, A.; Gayen, S.; Mishra, S.; Afsan, Z.; Vendier, L.; Ghosh, S. Borate ligand derived from CS_2 unveiling ruthenium dithioformate and trithia-borinane complexes. *Polyhedron* **2024**, *256*, 116986–116994. [CrossRef]
25. Ushijima, H.; Sudoh, S.; Kajitani, M.; Shimizu, K.; Akiyama, T.; Sugimori, A. Syntheses and electrochemical behaviour of novel dmit or dmio (dithiolato) cobalt(iii) complexes with a η^5-cyclopentadienyl or η^5-pentamethylcyclopentadienyl ring. *Appl. Organomet. Chem.* **1991**, *5*, 221–228. [CrossRef]
26. Adams, R.D.; Captain, B.; Kwon, O.-S.; Miao, S. New Disulfido Molybdenum-Manganese Complexes Exhibit Facile Addition of Small Molecules to the Sulfur Atoms. *Inorg. Chem.* **2003**, *42*, 3356–3365. [CrossRef]
27. Adams, R.D.; Captain, B.; Kwon, O.-S.; Pellechia, P.J.; Sanyal, S. Synthesis and properties of oligomers of iron–manganese carbonyl complexes with bridging disulfido ligands. *J. Organomet. Chem.* **2004**, *689*, 1370–1376. [CrossRef]
28. Jiang, F.; Siegler, M.A.; Sun, X.; Jiang, L.; Guerra, C.F.; Bouwman, E. Redox Interconversion between Cobalt(III) Thiolate and Cobalt(II) Disulfide Compounds. *Inorg. Chem.* **2018**, *57*, 8796–8805. [CrossRef]
29. Watanabe, L.K.; Ahmed, Z.S.; Hayward, J.J.; Heyer, E.; Macdonald, C.L.B.; Rawson, J.M. Oxidative addition of 1,2,5,6-Tetrathiocins to Co(I): A ReExamination of Crown Ether Functionalized Benzene Dithiolate Cobalt(III) Complexes. *Organometallics* **2022**, *41*, 226–234. [CrossRef]

30. Coucouvanis, D.; Patil, P.R.; Kanatzidis, M.G.; Detering, B.; Baenziger, N.C. Synthesis and Reactions of Binary Metal Sulfides. Structural Characterization of the $[(S_4)_2Zn]^{2-}$, $[(S_4)_2Ni]^{2-}$, $[(S_5)Mn(S_6)]^{2-}$, and $[(CS_4)_2Ni]^{2-}$ Anions. *Inorg. Chem.* **1985**, *24*, 24–31. [CrossRef]
31. Matsubayashi, G.; Akiba, K.; Tanaka, T. X-Ray molecular structures of $[Zn(C_3Se_5)_2]^{2-}$ and $[Zn(CSe_4)_2]^{2-}$ anion complexes. *J. Chem. Soc. Dalton Trans.* **1990**, 115–119. [CrossRef]
32. Huang, K.-C.; Tsai, Y.-C.; Lee, G.-H.; Peng, S.-M.; Shieh, M. Syntheses and X-ray Structures of a Series of Chalcogen-Containing Manganese Carbonylates $[E_2Mn_3(CO)_9]^-$, $[E_8C_2Mn_2(CO)_6]^{2-}$, and $[E_2Mn_4(CO)_{12}]^{2-}$ (E = Se, S). *Inorg. Chem.* **1997**, *36*, 4421–4425. [CrossRef]
33. Coucouvanis, D.; Draganjac, M.E.; Koo, S.M.; Toupadakis, A.; Hadjikyriacou, A.I. Reactivity of the $Mo(S_x)$ Functional Groups in Thio- and Oxothiomolybdate Complexes toward Carbon Disulfide. Synthesis and Reactivity of Trithio- and Perthiocarbonate Complexes of Mo(IV) and Mo(V) and Structural Characterization of *trans*-$[Ph_4P]_2[Mo(S)(CS_4)_2]$·DMF (I), *cis*-$[Ph_4Ppt_4N][Mo(S)(CS_4)_2]$ (II), *cis*-$[Ph_4P]_2[Mo_2(S)_2(M\text{-}S)_2(CS_4)_2]$·1/2DMF (III), *syn*-$[Ph_4P]_2[Mo_2(S)_2(M\text{-}S)_2(CS_3)_2]$ (IV), and *syn*-$[Et_4N]_2[Mo_2(O)_2(M\text{-}S)_2(CS_4)(CS_3)]$ (V). *Inorg. Chem.* **1992**, *31*, 1186–1196. [CrossRef]
34. Coucouvanis, D.; Fackler, J.P., Jr. Sulfur Chelates. IV.[1] Sulfur Addition to Dithiolato Complexes of Nickel(II). *J. Am. Chem. Soc.* **1967**, *89*, 1346–1351. [CrossRef]
35. Brunner, H.; Janietz, N.; Meier, W.; Sergeson, G.; Wachter, J.; Zahn, T.; Ziegler, M.L. $[(\eta^5\text{-}C_5Me_5)_2Fe_2S_4]$ and $[(\eta^5\text{-}C_5Me_5)_2Co_2S_4]$, Two Novel Bis(pentamethylcyclopentadienylmetal) Complexes Rich in Sulfur. *Angew. Chem. Int. Ed. Engl.* **1985**, *24*, 1060–1061. [CrossRef]
36. Brunner, H.; Janietz, N.; Wachter, J.; Nuber, B.; Ziegler, M.L. Die reaktion von $(C_5Me_5)_2Ru_2(CO)_4$ mit S_8, ein Beitrag zur synthese von ruthenium-polysulfidkomplexen. *J. Organomet. Chem.* **1988**, *356*, 85–91. [CrossRef]
37. Bianchini, C.; Mealli, C.; Meli, A.; Sabat, M. Stepwise Metal-assisted Conversion of CSe_2 to Se_2 and CO_2. Novel Bonding Mode of the Diselenium Molecule in the Double-Se_2-Bridged Complex $[(triphos)Rh(\mu\text{-}Se_2)_2Rh(triphos)](BPh_4)_2$.2DMF. *J. Am. Chem. Soc.* **1985**, *107*, 5317–5318. [CrossRef]
38. Kaur, U.; Saha, K.; Bairagi, S.; Das, A.; Roisnel, T.; Paine, T.K.; Ghosh, S. Structural and electronic analysis of bimetallic thiolate complexes of group-5 transition metal ions. *J. Organomet. Chem.* **2021**, *949*, 121943–121954. [CrossRef]
39. Govindaswamy, P.; Mozharivskyj, Y.A.; Kollipara, M.R. Syntheses, spectral and structural studies of Schiff base complexes of η^5-pentamethylcyclopentadienyl rhodium and iridium. *Polyhedron* **2005**, *24*, 1710–1716. [CrossRef]
40. Gennari, M.; Gerey, B.; Hall, N.; Pécaut, J.; Collomb, M.N.; Rouzières, M.; Clérac, R.; Orio, M.; Duboc, C. A Bio-Inspired Switch Based on Cobalt (II) Disulfide/Cobalt (III) Thiolate Interconversion. *Angew. Chem. Int. Ed.* **2014**, *126*, 5422–5425. [CrossRef]
41. Gennari, M.; Brazzolotto, D.; Yu, S.; Pécaut, J.; Philouze, C.; Rouzières, M.; Clérac, R.; Orio, M.; Duboc, C. Effect of the metal on disulfide/thiolate interconversion: Manganese versus cobalt. *Chem. Eur. J.* **2015**, *21*, 18770–18778. [CrossRef]
42. Atta, S.; Majumdar, A. Redox Convergent Synthesis and Reactivity of a Cobalt (III)-Pentasulfido Compound. *Chem. Eur. J.* **2023**, *29*, e202203579. [CrossRef]
43. Bhandari, A.; Mishra, S.; Maji, R.C.; Kumar, A.; Olmstead, M.M.; Patra, A.K. Nickel (II)-Mediated Reversible Thiolate/Disulfide Conversion as a Mimic for a Key Step of the Catalytic Cycle of Methyl-Coenzyme M Reductase. *Angew. Chem. Int. Ed.* **2020**, *59*, 9177–9185. [CrossRef]
44. Minami, K.; Kuwamura, N.; Yoshinari, N.; Konno, T. Controlled Formation of Thiol-Thiolate Hydrogen versus Disulfide Bonds between Two Iridium (III) Centers. *Chem. Asian J.* **2019**, *14*, 3291–3294. [CrossRef] [PubMed]
45. Abernethy, C.D.; Bottomley, F.; Decken, A.; Thompson, R.C. Organometallic Halides: Preparation and Physical and Chemical Properties of Tris[(η-pentamethylcyclopentadienyl)dichlorovanadium], $[(\eta\text{-}C_5Me_5)V(\mu\text{-}Cl)_2]_3$. *Organometallics* **1997**, *16*, 1865–1869. [CrossRef]
46. Sheldrick, G.M. *SHELXS-97*; University of Göttingen: Göttingen, Germany, 1997.
47. Sheldrick, G.M. Crystal structure refinement with SHELXL. *Acta Cryst.* **2015**, *C71*, 3–8. [CrossRef] [PubMed]
48. Dolomanov, O.V.; Bourhis, L.J.; Gildea, R.J.; Howard, J.A.K.; Puschmann, H.J. OLEX2: A complete structure solution, refinement and analysis program. *Appl. Crystallogr.* **2009**, *42*, 339–341. [CrossRef]
49. Frisch, M.J.; Trucks, G.W.; Schlegel, H.B.; Scuseria, G.E.; Robb, M.A.; Cheeseman, J.R.; Scalmani, G.; Barone, V.; Petersson, G.A.; Nakatsuji, H.; et al. *Gaussian 16, Revision C.01*; Gaussian, Inc.: Wallingford, CT, USA, 2016.
50. Lee, C.; Yang, W.; Parr, R.G. Development of the Colle-Salvetti correlation-energy formula into a functional of the electron density. *Phys. Rev. B Condens. Matter Mater. Phys.* **1988**, *37*, 785–789. [CrossRef] [PubMed]
51. Weigend, F.; Ahlrichs, R. Balanced basis sets of split valence, triple zeta valence and quadruple zeta valence quality for H to Rn: Design and assessment of accuracy. *Phys. Chem. Chem. Phys.* **2005**, *7*, 3297–3305. [CrossRef]
52. Weigend, F. Accurate Coulomb-fitting basis sets for H to Rn. *Phys. Chem. Chem. Phys.* **2006**, *8*, 1057–1065. [CrossRef] [PubMed]
53. Reed, A.E.; Curtiss, L.A.; Weinhold, F. Intermolecular Interactions from a Natural Bond Orbital, Donor-Acceptor Viewpoint. *Chem. Rev.* **1988**, *88*, 899–926. [CrossRef]
54. Weinhold, F.; Landis, C.R. *Valency and Bonding: A Natural Bond Orbital Donor-Acceptor Perspective*; Cambridge University Press: Cambridge, UK, 2005.
55. King, R.B. Topological Aspects of the Skeletal Bonding in "*Isocloso*" Metallaboranes Containing "Anomalous" Numbers of Skeletal Electrons. *Inorg. Chem.* **1999**, *38*, 5151–5153. [CrossRef]

56. King, R.B. Face-Localized Bonding Models for Borane Cage Ligands in Transition Metal Coordination Chemistry. *Inorg. Chim. Acta* **2000**, *300*, 537–544. [CrossRef]
57. Wiberg, K. Application of the Pople-Santry-Segal CNDO method to the cyclopropylcarbinyl and cyclobutylcation and to bicyclobutane. *Tetrahedron* **1968**, *24*, 1083–1096. [CrossRef]
58. Bader, R.F.W. *Atoms in Molecules: A Quantum Theory*; Oxford University Press: Oxford, UK, 1990.
59. Bader, R.F.W. A Bond Path: A Universal Indicator of Bonded Interactions. *J. Phys. Chem. A* **1998**, *102*, 7314–7323. [CrossRef]
60. Bader, R.F.W. A quantum theory of molecular structure and its applications. *Chem. Rev.* **1991**, *91*, 893–928. [CrossRef]
61. Lu, T.; Chen, F. Multiwfn: A multifunctional wavefunction analyzer. *J. Comput. Chem.* **2012**, *33*, 580–592. [CrossRef] [PubMed]
62. Dennington Keith, R.T.; Millam, J.; Eppinnett, K.; Hovell, W.L.; Gilliland, R. *GaussView*; Version 3.09, II; Semichem Inc.: Shawnee Mission, Kansas, 2003.
63. ChemCraft-Graphical Software for Visualization of Quantum Chemistry Computations. Available online: https://www.chemcraftprog.com (accessed on 29 November 2023).
64. Kaur, U.; Saha, K.; Raghavendra, B.; Ghosh, S. Role of Metals and Thiolate Ligands in the Structures and Electronic Properties of Group 5 Bimetallic–Thiolate Complexes. *Inorg. Chem.* **2020**, *59*, 12494–12503.
65. Weiss, R.; Grimes, R.N. Sources of Line Width in Boron-11 Nuclear Magnetic Resonance Spectra. Scalar Relaxation and Boron-Boron Coupling in B4H10 and B5H9. *J. Am. Chem. Soc.* **1978**, *100*, 1401–1405. [CrossRef]
66. Led, J.J.; Gesmar, H. Application of the linear prediction method to NMR spectroscopy. *Chem. Rev.* **1991**, *91*, 1413–1426. [CrossRef]